Draft version March 1, 2023
Typeset using LaTeX twocolumn style in AASTeX631

Deep Synoptic Array science: Two fast radio burst sources in massive galaxy clusters

Liam Connor,[1] Vikram Ravi,[1,2] Morgan Catha,[2] Ge Chen,[1] Jakob T. Faber,[1] James W. Lamb,[2] Gregg Hallinan,[1,2] Charlie Harnach,[2] Greg Hellbourg,[1,2] Rick Hobbs,[2] David Hodge,[1] Mark Hodges,[2] Casey Law,[1,2] Paul Rasmussen,[2] Jack Sayers,[1] Kritti Sharma,[1] Myles B. Sherman,[1] Jun Shi,[1] Dana Simard,[1] Jean Somalwar,[1] Reynier Squillace,[1] Sander Weinreb,[1] David P. Woody,[2] Nitika Yadlapalli,[1]

(The Deep Synoptic Array team)

[1] *Cahill Center for Astronomy and Astrophysics, MC 249-17 California Institute of Technology, Pasadena CA 91125, USA.*
[2] *Owens Valley Radio Observatory, California Institute of Technology, Big Pine CA 93513, USA.*

(Received; Revised; Accepted)

Submitted to ApJ Letters

ABSTRACT

The hot gas that constitutes the intracluster medium (ICM) has been studied at X-ray and millimeter/sub-millimeter wavelengths (Sunyaev–Zeld'ovich effect) for decades. Fast radio bursts (FRBs) offer an additional method of directly measuring the ICM and gas surrounding clusters, via observables such as dispersion measure (DM) and Faraday rotation measure (RM). We report the discovery of two FRB sources detected with the Deep Synoptic Array (DSA-110) whose host galaxies belong to massive galaxy clusters. In both cases, the FRBs exhibit excess extragalactic DM, some of which likely originates in the ICM of their respective clusters. FRB 20220914A resides in the galaxy cluster Abell 2310 at $z = 0.1125$ with a projected offset from the cluster center of 520±50 kpc. The host of a second source, FRB 20220509G, is an elliptical galaxy at $z = 0.0894$ that belongs to the galaxy cluster Abell 2311 at projected offset of 870±50 kpc. These sources represent the first time an FRB has been localized to a galaxy cluster. We combine our FRB data with archival X-ray, SZ, and optical observations of these clusters in order to infer properties of the ICM, including a measurement of gas temperature from DM and y_{SZ} of 0.8–3.9 keV. We then compare our results to massive cluster halos from the IllustrisTNG simulation. Finally, we describe how large samples of localized FRBs from future surveys will constrain the ICM, particularly beyond the virial radius of clusters.

Keywords: galaxy clusters — radio transient sources, Abell 2310, Abell 2311

1. INTRODUCTION

Galaxy clusters are massive ($10^{14} - 10^{15}\,M_\odot$) gravitationally bound objects comprised of hundreds to thousands of galaxies. Galaxies make up just a few percent of the total cluster mass. The dominant component of baryons by mass and volume is in the hot intracluster medium (ICM) made of diffuse gas with $n_e \approx 10^{-3}\,\mathrm{cm}^{-3}$ and $T_e \approx 10^7 - 10^8\,\mathrm{K}$. Within a sufficiently large volume (e.g., the virial radius), the ratio of dark matter to baryons approximately matches the Universal value (Eckert et al. 2019), which is not true for smaller halos where feedback is expected to expel gas beyond the virialized dark matter halos (Tumlinson et al. 2017).

The ICM has been studied in great detail at X-ray wavelengths for the past fifty years (Sarazin 1986). Thermal bremsstrahlung emission from gas heated to 2–15 keV is observed out to the virial radii of clusters (1–2 Mpc), tracing the radial distribution of the ICM gas (Ghirardini et al. 2019). The ICM reaches such high temperatures by adiabatic compression and shock heating as the gas reaches hydrostatic equilibrium within the potential well (Voit 2005). Free-free emission scales

Corresponding author: Liam Connor
liam.dean.connor@gmail.com

with emissivity, and the specific X-ray luminosity can be written as an integral of plasma density squared,

$$L_X \approx \int n_e^2\, \Lambda(T_e)\, \mathrm{d}V, \tag{1}$$

where n_e is the number density of free electrons and $\Lambda(T_e)$ characterizes the temperature dependence of X-ray emission. The total mass can then be inferred from the cluster's X-ray luminosity (Pratt et al. 2009a). X-ray spectroscopy can also be used to measure the gas temperature (Böhringer & Werner 2010) and its velocity structure (Hitomi Collaboration et al. 2016).

The hot plasma in the ICM is also observable at millimeter/sub-millimeter wavelengths through the thermal Sunyaev-Zel'dovich (SZ) effect, whereby photons in the cosmic microwave background (CMB) are inverse Compton scattered by thermal electrons (Mroczkowski et al. 2019). This leads to spectral distortions in the CMB at the level of 10^{-4}–10^{-5}. SZ observations of the ICM are parameterized by the Compton Y-parameter, which is given by the integral of electron thermal pressure along the line of sight,

$$y_{SZ} = \frac{k_B\, \sigma_T}{m_e\, c^2} \int n_e\, T_e\, \mathrm{d}l, \tag{2}$$

where k_B is Boltzmann's constant, σ_T is the Thomson cross-section, m_e is electron mass, c is the speed of light.

Fast radio bursts (FRBs) offer an additional probe of the ICM of massive galaxy clusters. FRBs are short-duration (10^{-2}–10^{2} ms) radio transients that have been detected over cosmological distances ($z \lesssim 1.5$) (Petroff et al. 2019; Cordes & Chatterjee 2019). To date, $\mathcal{O}(10^3)$ sources have been discovered (CHIME/FRB Collaboration et al. 2021; Petroff et al. 2016) but only two-dozen have been localized with sufficient angular precision to identify a host galaxy (Chatterjee et al. 2017; Ravi et al. 2019; Heintz et al. 2020; Bhandari et al. 2020). Propagation effects imparted on the radio pulse encode information about the plasma through which the burst travelled. Dispersion measure (DM) is an integral of line-of-sight electron density and is given by,

$$\mathrm{DM} = \int n_e\, \mathrm{d}l. \tag{3}$$

Unlike with thermal X-ray emission or SZ observations of the ICM, the FRB DM is detectably impacted by *all* plasma between us and the source, not just 10^{6-8} K gas. This is both a blessing and a curse: FRB DMs will probe plasma in the host galaxy, the circumgalactic medium (CGM), the ICM of intervening or host clusters, the intergalactic medium (IGM), and the Milky Way's interstellar medium (ISM). For individual FRB sightlines, these terms must be explicitly modelled. An FRB that is impacted by a galaxy cluster will have the following "DM budget",

$$\mathrm{DM_{obs}} = \mathrm{DM_{MW}} + \mathrm{DM_{IGM}} + \frac{\mathrm{DM_{ICM}}}{1+\mathrm{z_c}} + \frac{\mathrm{DM_{host}}}{1+\mathrm{z_{frb}}}, \tag{4}$$

where z_c and z_{frb} are the cluster and FRB redshifts, respectively. The observed DM is likely dominated by the IGM for most FRBs. Still, it is important to be specific about what is meant by the IGM. In Macquart et al. (2020), the relationship between $\mathrm{DM_{cosmic}}$ and source redshift includes all extragalactic gas between the Milky Way and the host galaxy. $\mathrm{DM_{cosmic}}$ therefore includes the CGM, intragroup medium (IGrM), ICM, and IGM. All of those terms correlate with source distance because the optical depth of halos increases with redshift. In this work we take the IGM to be ionized gas that resides outside of virialized dark matter halos (McQuinn 2016).

For sources that intersect or are embedded in galaxy clusters, the largest DM contribution may be from the ICM (Prochaska & Zheng 2019). For example, a cluster with $\langle n_e \rangle = 10^{-3}\,\mathrm{cm^{-3}}$ and $R_{200} = 1\,\mathrm{Mpc}$ will lead to $\mathrm{DM_{ICM}} \sim 10^3\,\mathrm{pc\,cm^{-3}}$ for low impact parameters. This value is more than double the typical contribution from the IGM for a source at $z = 0.5$ and 70% larger than the mean DM_{obs} of CHIME/FRB sources (Macquart et al. 2020; CHIME/FRB Collaboration et al. 2021). The polarization properties of FRBs can help measure the magnetic field of the ICM. Faraday rotation measure (RM) is an integral of the free electrons, weighted by the line-of-sight magnetic field strength,

$$\mathrm{RM} = \frac{e^3}{2\pi\, m_e^2\, c^4} \int B_\parallel\, n_e(l)\, \mathrm{d}l, \tag{5}$$

where e is the charge of an electron. While other radio objects can provide cluster RMs (van Weeren et al. 2019), FRBs are unique amongst extragalactic sources in their ability to measure both RM and DM. Therefore, if one can isolate the components of RM and DM that are due to the ICM, the mean line-of-sight magnetic field strength in the cluster can be determined by their ratio,

$$\langle B_{\parallel,\mathrm{ICM}} \rangle = 1.23\,\mu\mathrm{G}\, \frac{\mathrm{RM_{ICM}}}{\mathrm{DM_{ICM}}}, \tag{6}$$

where RM and DM are given in the standard units of $\mathrm{rad\,m^{-2}}$ and $\mathrm{pc\,cm^{-3}}$, respectively. The application of FRBs to the ICM has been considered in previous works, including the detection of an FRB in the direction of the Virgo cluster by ASKAP (Agarwal et al. 2019). In that case, the localization precision was insufficient to determine a host galaxy, so it was unclear if the source was

embedded in, or behind, the cluster. Another unlocalized source, FRB 20190116A (CHIME/FRB Collaboration et al. 2019) is likely within a ∼ 5 Mpc of the Coma cluster in projection and may be dispersed by filamentary structure extending from the cluster (Hallinan et al. 2019a). Fujita et al. (2017) investigated the application of FRBs to the warm hot intergalactic medium (WHIM) at the outskirts of galaxy clusters, where X-ray observations are difficult due to the n_e^2 dependence of emissivity. Nonetheless, most of the effort in studying halo gas with FRBs has been devoted to the circumgalactic medium (Prochaska & Zheng 2019; Ravi 2019; Lee et al. 2022). That is because the CGM is more difficult to detect than the ICM using traditional means (X-ray and SZ observations are much less sensitive to the gas in galaxy-scale halos), and because of the CGM's significance in galaxy formation and feedback processes. Connor & Ravi (2022) presented the first statistical evidence for the impact of halo gas on FRBs and demonstrated the importance of considering galaxy groups on FRB DM budgets. As we demonstrate, current and future FRB surveys will find a significant number of sources that are impacted by galaxy clusters, and understanding their effects and prevalence are important for CGM studies, in addition to studying the ICM itself.

In this work we make the first unambiguous detection of FRB sources that belong to a galaxy cluster. Both sources were discovered by the real-time FRB survey on the Deep Synoptic Array (DSA-110)[1]. The DSA-110 is a radio interferometer at the Owens Valley Radio Observatory (OVRO) that was built to localize FRBs with ∼ arcsecond precision. A detailed account of the instrument will be presented in Ravi et al. (in prep.). During the observations presented in this work, the DSA-110 was operating in its commissioning phase with 63 antennas collecting data, as described in Ravi et al. (2022).

In Section 2 we describe the radio properties of two FRBs using the DSA-110. We describe the two massive clusters of which the FRB host galaxies are members. A companion paper details the interferometric localizations of FRB 20220509G and FRB 20220914A as well as their unusual host galaxies (Sharma et al., in prep.). In Section 3.2 we model the DM contribution from the ICM for both sources, combining our radio data with archival X-ray, SZ, and optical data to infer properties about the clusters' respective ICM. Finally, we compare our results with clusters found in the IllustrisTNG simulation.

[1] https://deepsynoptic.org

2. CLUSTER FRBS

The radio properties of FRB 20220914A and FRB 20220509G are listed in Table 1. The observed parameters of their respective host galaxy clusters are given in Table 2. The two FRBs presented here are from distinct galaxy clusters, but are relatively nearby on the sky—separated by just 3.1 degrees. DSA-110 is a transit instrument that was parked at Declination ∼ +70 for most of the 2022 commissioning period. For this reason, most of our initial sample of sources fall on a ring in RA and several pairs are within a few degrees of each other. Below we described observations of the FRBs and their host galaxies, as well as archival data obtained for the galaxy clusters.

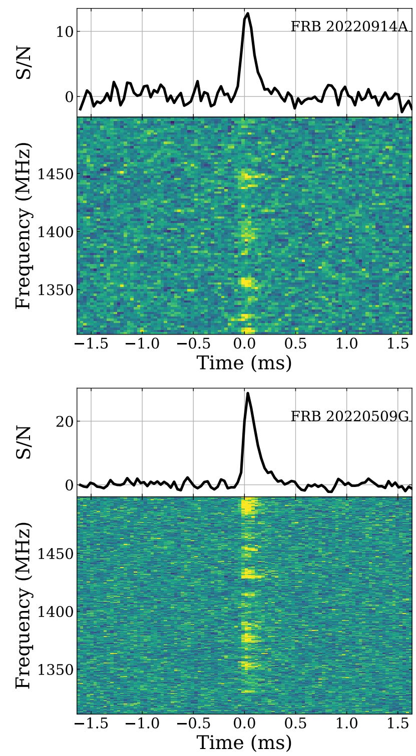


Figure 1. Dedispersed total-intensity dynamic spectra for two FRBs detected by DSA-110. Both FRBs reside in galaxies that belong to massive galaxy clusters.

2.1. *FRB 20220914A*

FRB 20220914A was detected at MJD 59836.1459660. Follow-up analysis found an optimal DM of 631.3 pc cm^{-3} and a pulse full-width at half maximum (FWHM) of 140 μs. With a S/N of 13.4 and system-equivalent flux density (SEFD) of 140 Jy, the fluence of the burst was roughly 2.2 Jy ms. Offline interferometric localization found the position of the FRB to be R.A. J2000, decl. J2000 = 18h48m13.63s, +73d20m12.89s,

Source	RA (deg)	Dec (deg)	z_{gal}	DM_{obs}	DM_{MW}	RM_{obs}	τ (ms)	$\mathcal{F}$ (Jy ms)	$b_{\perp}$ (kpc)
FRB 20220914A	282.0568	73.3369	0.1139	631.29	47/55	N/A	< 0.080	2.2	520±50
FRB 20220509G	282.6700	70.2438	0.0894	269.53	46/55	−110(1)	0.08±0.02	5.5	870±50

Table 1. The radio properties of two galaxy cluster FRBs. DM and RM are reported in $\mathrm{pc\,cm^{-3}}$ and $\mathrm{rad\,m^{-2}}$, respectively. The scattering timescale, τ, is referenced to 1.4 GHz. The two Galactic ISM DM estimates listed are YMW16 and NE2001. RA and Dec are in epoch J2000.

Cluster	RA (deg)	Dec (deg)	Richness	z_{clust}	M_{500} ($M_{\odot}$)	R_{500} (kpc)	L_X (erg/s)	Y_{5R500} (arcmin^2)
Abell 2310	281.81708	73.3472	124	0.1125	1.7×10^{14}	810	8.3×10^{43}	$0.85\pm0.35\times10^{-3}$
Abell 2311	282.497	70.376	190	0.0899(1)	1.6×10^{14}	800	4.7×10^{43}	$0.81\pm0.36\times10^{-3}$

Table 2. The properties of two galaxy clusters that host the FRBs presented in this paper. L_X is the X-ray luminosity at 0.1–2.4 keV within R_{500}.

the centroid of which is 1.6" from a galaxy with spectroscopic redshift $z = 0.1139$. The expected DM from the Milky Way at these Galactic coordinates is roughly $50\,\mathrm{pc\,cm^{-3}}$ from NE2001 (Cordes & Lazio 2002) and $47\,\mathrm{pc\,cm^{-3}}$ from YMW16 (Yao et al. 2017). The IGM is expected to contribute 50–120 $\mathrm{pc\,cm^{-3}}$ at this redshift, suggesting that FRB 20220914A has significant extragalactic DM excess.

We find no evidence of scattering, placing an upper-limit of $\tau < 80\,\mu$s at 1.4 GHz. Polarimetric analysis found no detectable polarization and no RM was determined after searching a range of -10^6 to $+10^6\,\mathrm{rad\,m^{-2}}$. The upper-limits on polarization fraction were $L/I <$ 15% and $V/I <$ 20%.

2.1.1. *ABELL 2310 galaxy cluster*

The position of FRB 20220914A was cross-matched with both the DESI Legacy Imaging Surveys Data Release 9 (DR9) galaxy catalog (Dey et al. 2019) and DR9 cluster/group catalog (Yang et al. 2021). We find that the host galaxy of FRB 20220914A is a member of the massive galaxy cluster Abell 2310 (Abell 1958). According to the DESI DR9 group/cluster catalog, this cluster has richness 124 (i.e. number of member galaxies), $M_{180} = 2.5 \times 10^{14}\,M_{\odot}$, with a brightest cluster galaxy (BCG) at spectroscopic redshift $z = 0.1125$. The cluster is also in the Meta-Catalog of X-Ray Detected Clusters of Galaxies (MCXC) with source name J1847.2+7320 (Piffaretti et al. 2011). The X-ray surface brightness centroid is at 18h47m16.s 73d20m50s (Piffaretti et al. 2011). The FRB offset from this position is 4.22' suggesting a projected physical impact parameter of 520 kpc. The X-ray luminosity within R_{500} is $8.31\times10^{43}\,\mathrm{erg\,s^{-1}}$, which gives $M_{500} = 1.69 \times 10^{14}\,M_{\odot}$ using an empirical $L_X - M$ relation (Pratt et al. 2009b; Piffaretti et al. 2011).

The cluster has also been detected via the thermal SZ effect and is listed in the Planck SZ2 cluster catalog as PSZ2 G104.29+26.17 (Planck Collaboration et al. 2016a). The SZ-derived mass based on a hydrostatic mass calibration is $M_{500} = 1.94 \pm 0.28 \times 10^{14}\,M_{\odot}$ (Planck Collaboration et al. 2014), and its SZ centroid has a physical offset from FRB 20220914A of ~ 380 kpc. We have also analyzed the Planck MILCA y-map from Planck Collaboration et al. (2016b) using the techniques described in Sayers et al. (2016) to obtain both a two-dimensional projected model of the cluster $y(\theta)$, along with the total integrated SZ signal Y_{5R500}. In brief, we assume the cluster follows the profile shape given by Arnaud et al. (2010), with the scale radius set by the X-ray value of R_{500} and centered on the X-ray centroid. We then determine the best-fit normalization of this model, with the uncertainty on this normalization estimated from fits to 100 random realizations of the Planck noise. The result is $Y_{5R500} = 0.85 \pm 0.35$ arcmin^2.

The point-spread function (PSF) of Planck is large, so we take the offset between FRB 20220914A and Abell 2310 to be the separation between the X-ray centroid and the FRB's host galaxy. This gives a projected physical offset of 520±50 kpc. In Figure 4 we show the filtered X-ray data with a contour for the SZ emission region, as well as a zoom in on the optical host galaxy image. The X-ray intensity data is taken from the public archive of X-ray clusters[2] (Xu et al. 2022).

The redshift difference between the host galaxy of FRB 20220914A and the brightest cluster galaxy (BCG) is $\Delta z = -0.00129$, indicating the host has a recession velocity of roughly $390\,\mathrm{km\,s^{-1}}$. We do not know the radial position of the FRB within the cluster, but we have good reason to believe it is not near the front. We take

[2] https://github.com/wwxu/rxgcc.github.io

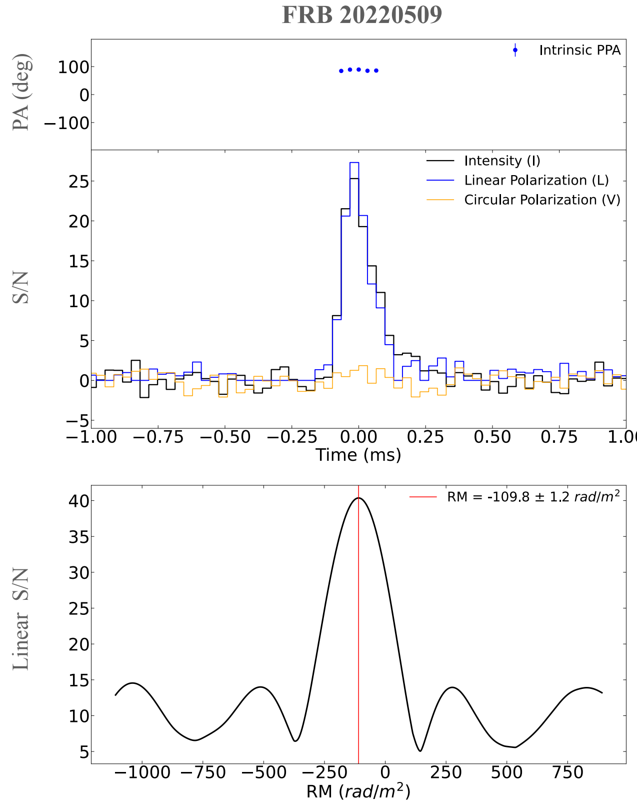


Figure 2. The polarization properties of FRB 20220509G. The top panel shows a flat PA across the pulse and the middle panel shows the linearly polarized pulse profile. The bottom panel is the Faraday spectrum with a peak at RM=$-111.5\,\mathrm{rad\,m^{-2}}$.

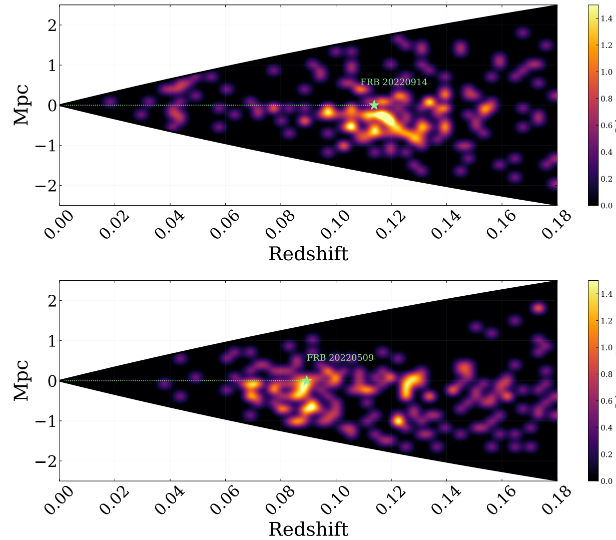


Figure 3. Slice plots of the smoothed galaxy number density within 5 arcminutes of each FRB line-of-sight. The galaxy data are from the DESI Legacy Imaging Survey DR9 and are mostly photometric redshifts.

the radial position to be l_{LOS}, which is zero at the distance of the cluster center and negative behind the cluster. The radial distribution of galaxies in clusters is well described by an NFW profile with concentration parameter c=2.6 (Budzynski et al. 2012). With a virial radius of 800 kpc, the probability distribution of galaxy radius peaks around 300 kpc and declines towards larger radii. Therefore, for an impact parameter beyond 300 kpc, the most likely l_{LOS} is zero. More convincingly, as we show in Section 3.2, the FRB has significant excess dispersion that likely comes from the ICM. The magnitude of this extra DM cannot easily be explained by the IGM or the host galaxy, so l_{LOS} is likely smaller than several hundred kpc.

2.1.2. *The host galaxy of FRB 20220914A*

The FRB 20220914 has been localized to a typical late-type spiral galaxy at R.A. (J2000) = 18:48:13.9580 and declination (J2000) = +73:20:10.703 (Sharma et al., in prep.). The spectroscopic redshift of the galaxy, as measured from optical spectra acquired with Keck-I/LRIS, is 0.1139 ± 0.0001. A detailed spectral energy distribution analysis revealed a stellar mass of $\log M_*(M_\odot) = 9.99^{+0.09}_{-0.09}$. The constrained star formation history indicates significant recent star formation with several starbursts over the last 3.5 Gyr, thus reflecting a wide probability distribution for the age of its progenitor.

2.2. *FRB 20220509G*

The fast radio burst source FRB 20220509G had an arrival time of 59708.4944991 at reference frequency of 1500 MHz. Its optimal DM was $269.53\,\mathrm{pc\,cm^{-3}}$ and had a fluence of 5.5 Jy ms. Offline interferometric localization found that the source is at R.A. J2000, decl. J2000 = 18h50m40.8s, +70d14m37.8, with a 90% error ellipse with axes 4.7 and 3.2 in R.A. and decl. This is within 6" of a massive galaxy with spectroscopic redshift $z = 0.0894$. The Galactic ISM DM estimates are $55\,\mathrm{pc\,cm^{-3}}$ from NE2001 and $46\,\mathrm{pc\,cm^{-3}}$ from YMW16. The expected IGM contribution at this redshift is roughly $75\,\mathrm{pc\,cm^{-3}}$, but with significant uncertainty. We analyze the source's DM budget in Section 3.2. The burst was fit with a scattering tail plus a Gaussian component. We find evidence of scattering with a timescale of $80{\pm}20\,\mu$s at 1.4 GHz and a Gaussian component that is $30 \pm 10\,\mu$s. Offline polarimetric analysis found that FRB 20220509G was nearly 100% linearly polarized with an RM of $-111.5 \pm 1.5\,\mathrm{rad\,m^{-3}}$ in the observer frame. This is significantly larger than the Galactic RM foreground value of $-9 \pm 16\,\mathrm{rad\,m^{-3}}$. The burst's position angle (PA) is flat across the pulse. The

polarization properties of FRB 20220509G are shown in Figure 2.

2.2.1. *Abell 2311 galaxy cluster*

The host galaxy of FRB 20220509G is a member of the galaxy cluster Abell 2311 (Abell 1958). According to the DESI DR9 cluster/group catalog, the cluster's richness is 190 with $M_{180} = 2.5 \times 10^{14}\, M_\odot$, determined by the velocity dispersion of member galaxies. The radius at which the average enclosed density is 500 times the critical density is $R_{500} = 800$ kpc. The X-ray luminosity within R_{500} is $L_X = 4.7 \times 10^{43}\,\mathrm{erg\,s^{-1}}$ with an inferred mass of $M_{500} = 1.6 \times 10^{14}\, M_\odot$. The cluster does not have a published SZ detection and is not in the Planck SZ2 cluster catalog. However, we have analyzed the Planck MILCA y-map for this cluster in the same way as for Abell 2311, finding $Y_{5R500} = 0.81 \pm 0.36 \times 10^{-3}$ arcmin^2.

The filtered ROSAT X-ray intensity is shown in Figure 4. The projected physical offset between FRB 20220509G and the X-ray centroid is 870 ± 50 kpc, placing the FRB at a minimum radius of just beyond R_{500}.

2.2.2. *The host galaxy of FRB 20220509G*

The likely host galaxy of FRB 20220509 is an early-type elliptical galaxy with insignificant ongoing star formation, and hence stands out as a quiescent galaxy in the known population of FRB hosts (Sharma et al., in prep.). The measured spectroscopic redshift of the host is 0.0894 ± 0.0001 and a detailed spectral energy distribution analysis reveals a stellar mass of $\log \mathrm{M}_*(\mathrm{M}_\odot) = 11.13^{+0.02}_{-0.02}$ with star formation rate averaged over the last 100 Myr of $0.08^{+0.06}_{-0.04}$. An old stellar population implies a long delay between the time of occurrence of this FRB and the formation of its progenitor, thus opening another window of progenitors with long delay times.

3. DATA ANALYSIS

We now seek to synthesize the FRB radio properties with observations of their host galaxies and host clusters. This will allow us to infer the impact of the ICM on FRB 20220509G and FRB 20220914A. Neither host galaxy has a high rate of star formation. The early-type host of FRB 20220509G, in particular, is not expected to have a significant ISM that would contribute to local dispersion (Lees 1992). In this section we estimate the origin of scattering, DM, and RM and model the contribution of the ICM to each propagation effect.

3.1. *Scattering & scintillation*

Both FRB sources show evidence of scintillation that is consistent with a nearby scattering screen in the Milky Way. FRB 20220509G and FRB 20220914A have decorrelation bandwidths of $\Delta\nu = 3.1 \pm 0.7$ MHz and $\Delta\nu = 2.51 \pm 0.16$ MHz, respectively. Since the two sources are only separated by a few degrees, it is unsurprising that their decorrelation bandwidth and modulation indexes are similar. However, the presence of fully-modulated scintillation is physically interesting in the case of FRB 20220509G, which also shows evidence of temporal scattering. The presence of both scattering and spectral scintillation allows one to place constraints on the geometry of the two scattering screens. Scattering causes angular broadening and if that broadening were too large the FRB would be resolved out by the scattering screen in our Galaxy (Masui et al. 2015; Connor et al. 2016; Simard & Ravi 2021).

For a given scattering timescale, angular broadening is maximal when the screen is halfway between us and the source. Therefore, if the screen were in the CGM of an intervening galaxy at $z \sim 0.05$, we would not expect FRB 20220509G to scintillate. Following Eq 48 in Simard & Ravi (2021), we place an upper-limit on the distance between the FRB source and the first scattering screen to be ≤ 140 kpc. This leads to three scenarios for the origin of the temporal scattering in FRB 20220509G, each of which is plausible but somewhat surprising given the early-type host galaxy and the hot, smooth ICM in which it is embedded. The scattering could be in the ISM of the host galaxy at $\sim$kpc scales from the FRB emitting source. This would require an unusual sightline given the lack of Hα emission and limited turbulence in the ISM of elliptical galaxies (Seta et al. 2021; Ocker et al. 2022). Alternatively, it could arise in the immediate vicinity of the source, such as in a stellar wind, analogous to the scattering in FRB 20190520 (Niu et al. 2022a; Ocker et al. 2023; Beniamini et al. 2022; Anna-Thomas et al. 2022). A third option is that it could be near the host galaxy in the ICM, perhaps in the outflows or CGM of the host.

3.2. *DM from the ICM*

We model the DM along the line of sight to each FRB in order to generate a probability distribution for the ICM contribution. The probability density function (PDF, denoted here by $\mathcal{P}$) of a sum of independent variables is the convolution of their individual PDFs. The DM terms are not strictly independent, but we find that the convolution relation for a sum of variables is a good approximation in this case. Using Eq. 4, we find,

$$\mathcal{P}(\mathrm{DM_{ICM}}) = \mathcal{P}(\mathrm{DM_{obs}}) * \mathcal{P}(-\mathrm{DM_{MW}}) * \mathcal{P}(-\mathrm{DM_{IGM}}) * \mathcal{P}(-\mathrm{DM_h}) \quad (7)$$

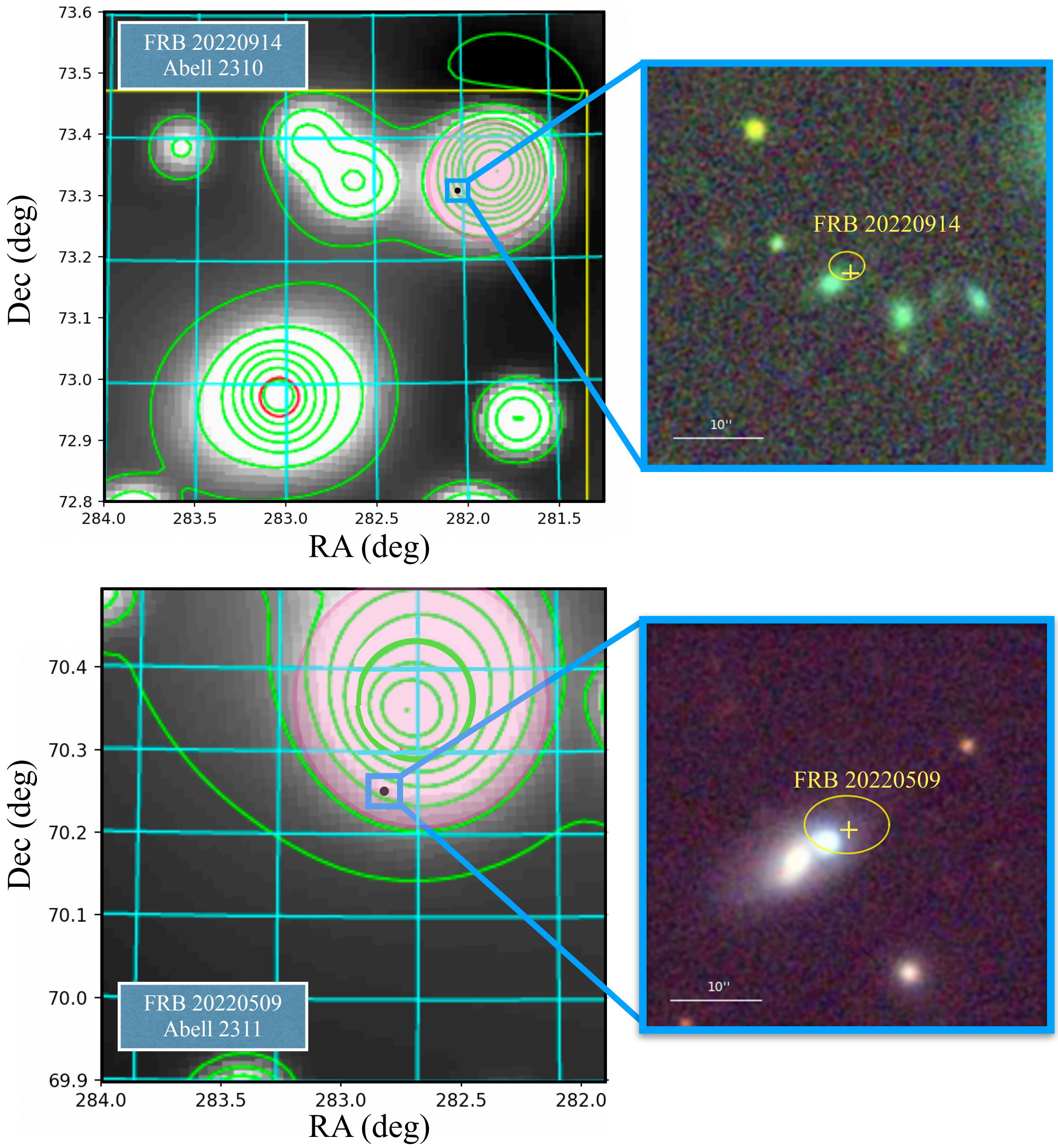


Figure 4. The two FRB sources reported in this work with their respective host galaxies and galaxies clusters. The left column images show filtered ROSAT X-ray intensity (Xu et al. 2022) for galaxy cluster Abell 2310 (top) and Abell 2311 (bottom). The magenta circle in the top left panel has a radius of 1 Mpc and denotes the location of the SZ cluster from the PSZ2 catalog. The bottom panel magenta cirlce corresponds to our SZ measurement for Abell 2311. The right columns show insets on the position of FRB 20220914A (top) and FRB 20220509G (bottom) plotted over a PanSTARRS1 riz-band image (Chambers et al. 2016, PS1).

where $\mathcal{P}(\mathrm{DM_{obs}})$ is Gaussian with variance determined by the measurement error on the observed DM. Here the DMs are all in the observer frame, so we must multiply by $1 + z_c$ when estimating the DM from the ICM. We assert that the probability density must be zero for negative DM.

For FRB 20220914A, we place an upper-limit on $\mathrm{DM_h}$ to be $50\,\mathrm{pc\,cm^{-3}}$ based on the strong upper limit on temporal scattering. We take $\mathcal{P}(\mathrm{DM_h})$ to be a uniform distribution between 0 and $50\,\mathrm{pc\,cm^{-3}}$ because we do not have a strong motivation for a preferred DM peak in the distribution. Previous detections of unscattered FRBs do not have a robust measurement of local DM on which to base an empirical distribution.

There is reason to believe the local DM contribution is very small for other similar FRB sources. For example, FRB 20180916B (Pastor-Marazuela et al. 2021) and FRB 20220319D (Ravi et al. 2023) have comparable upper-limits on local scattering and likely have $\mathrm{DM}_h \leq 20\,\mathrm{pc\,cm^{-3}}$. The local ($< 150$ kpc) contribution to the DM of FRB 20220509G is less certain, due to the presence of both scattering and scintillation. We assume a flat prior between 0 and $100\,\mathrm{pc\,cm^{-3}}$.

For $\mathcal{P}(\mathrm{DM_{IGM}})$, we use the IllustrisTNG simulation to estimate the distribution of DM from the IGM for a source at a few hundred Mpc along similar sightlines to our FRBs. We take the functional form of $\mathrm{DM_{IGM}}$ found by Zhang et al. (2021) for FRBs at $z \approx 0.1$, who also used IllustrisTNG. However, we independently estimate the mean $\mathrm{DM_{IGM}}$ for sightlines that intersect massive halos with $M_{500} > 10^{13.5}\,M_\odot$. We then exclude DM contribution from the halo itself to estimate the mean of $\mathrm{DM_{IGM}}$ for that subset of sightlines. By doing this we account for correlations in the Universe's matter distribution: Sightlines that intersect clusters are more likely to intersect filaments and less likely to pass through voids, compared to typical positions. We find that for $z \lesssim 0.1$,

$$\langle \mathrm{DM_{IGM}} \rangle \approx 22\,\mathrm{pc\,cm^{-3}} \left(\frac{\mathrm{D_A}}{100\,\mathrm{Mpc}} \right), \tag{8}$$

where D_A is angular diameter distance. This gives a mean value of $93\,\mathrm{pc\,cm^{-3}}$ with a 90% confidence interval on $\mathrm{DM_{IGM}} = 48 - 260\,\mathrm{pc\,cm^{-3}}$ for FRB 20220914A. For FRB 20220509G we find a mean value of $76\,\mathrm{pc\,cm^{-3}}$ with a 90% confidence interval on $\mathrm{DM_{IGM}} = 39 - 175\,\mathrm{pc\,cm^{-3}}$. The estimated IGM DM distributions are shown in Figure 5 as dashed red curves.

In these FRB directions, the Milky Way contribution is taken to be normally distributed with mean $70\,\mathrm{pc\,cm^{-3}}$ and standard deviation $30\,\mathrm{pc\,cm^{-3}}$. This value includes the Galactic halo. These values are based on NE2001 (Cordes & Lazio 2002) and YMW (Yao et al. 2017) and recent evidence that the Milky Way halo contribution to DM is smaller than previously thought (Bhardwaj et al. 2021; Ravi et al. 2023; Cook et al. 2023). The two FRB sources are nearby on the sky, allowing us to use similar estimates for $\mathcal{P}(\mathrm{DM_{MW}})$.

We have attempted to make conservative estimates on the uncertainty of each component of the observed DM, which will result in a wider inferred $\mathrm{DM_{ICM}}$ distribution. We warn that the various elements in the DM budget were estimated by different means and are subject to modelling uncertainties. With these caveats, the resulting probability distribution of the ICM contribution to DM is shown in Figure 5. We find that Abell 2310's ICM adds 265–511 $\mathrm{pc\,cm^{-3}}$ at 90% confidence to the observed DM of FRB 20220914A. In the frame of the cluster, this range is 295–568 $\mathrm{pc\,cm^{-3}}$. These values make it unlikely that the host galaxy is near the front of the cluster, as such a high $\mathrm{DM_{ICM}}$ requires a significant path through the intracluster medium. In the case of Abell 2311, we find a 90% confidence interval of 16–172 $\mathrm{pc\,cm^{-3}}$ for $\mathrm{DM_{ICM}}$ in the cluster frame. This range is consistent with an FRB embedded in a $1.6 \times 10^{14}\,M_\odot$ cluster at a projected offset of $\sim$870 kpc. Still, it is difficult to say with certainty that the FRB's majority DM component is the ICM due to the presence of scattering and larger projected impact parameter of the host.

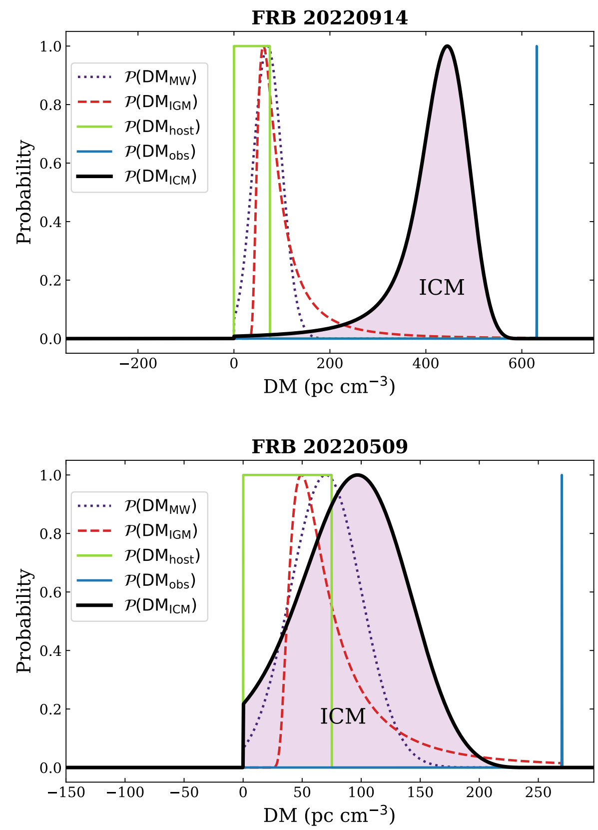


Figure 5. The relative probability distributions for each component of the observed FRB DMs. The distributions of $\mathrm{DM_{ICM}}$ are shown in the purple shaded region under the black curves.

3.3. *ICM magnetic field*

FRBs are the only known cosmological sources for which both DM and RM can be measured. If $\mathrm{DM_{ICM}}$ and $\mathrm{RM_{ICM}}$ can be determined, FRBs allow us to measure the mean line-of-sight magnetic field strength of a galaxy cluster, as shown in Eq. 6. The observed

RM of FRB 20220509G is $-111.5 \pm 1\,\mathrm{rad\,m^{-2}}$, compared with the expected Milky Way foreground RM of $-9 \pm 16\,\mathrm{rad\,m^{-2}}$ in that direction (Hutschenreuter et al. 2022). If the extragalactic RM is dominated by the ICM then the cluster-frame RM is $\approx 120\,\mathrm{rad\,m^{-2}}$, and we can use $\mathcal{P}(\mathrm{DM_{ICM}})$ to infer $\langle B_{\parallel,\mathrm{ICM}}\rangle$ at the impact parameter of FRB 20220509G. We find that the average magnetic field strength is 0.7–7.5 μG. Again, this is subject to the assumption that the observed RM is dominated by the ICM.

The values we obtain for both RM and $\langle B_{\parallel,\mathrm{ICM}}\rangle$ are in line with previous observations, as well as magnetohydrodynamical (MHD) simulations of galaxy clusters (Carilli & Taylor 2002; Marinacci et al. 2018). Böhringer et al. (2016) analyzed the RMs from 1383 of extragalactic polarized sources and found values between -200 and $+200\,\mathrm{rad\,m^{-2}}$ were common at R_{500}. The corresponding magnetic field strengths they deduced were $\sim$ a few microGauss (Böhringer et al. 2016). In Section 5 we discuss how cluster FRBs from future surveys could better constrain magnetic fields in and around the ICM.

3.4. *Mean temperature from DM*

The ICM observables that we discuss in this work are DM, RM, X-ray brightness, and the SZ-y parameter. Each is a weighted integral of n_e along the line of sight. In Faraday rotation, the gas density is weighted by magnetic field strength, $B_{//}$. For X-ray luminosity, emission is the sum of n_e^2 weighted by $\Lambda(T_e)$. In the case of the SZ-y parameter, n_e is weighted by T_e itself. X-ray derived density and SZ-derived pressure are commonly used to estimate temperature (Eckert et al. 2013). Alternatively, the ratio of X-ray luminosity to y_{SZ} has been taken to constrain the gas temperature. For example, Planck Collaboration et al. (2016c) find the ratio of X-ray luminosity to y_{SZ} for the Virgo cluster at angular position θ to be $\langle n_e\,\Lambda(T_e)/(k_B\,T_e)\rangle(\theta)$. This quantity offers information on the cluster temperature profile under certain assumptions about $n_e(r)$ and Λ.

We can attempt something similar using the ratio of y_{SZ} to $\mathrm{DM_{ICM}}$, which will be independent of n_e. Evaluating Eq. 2 and Eq. 3 at impact parameter $b_\perp$ we get,

$$y_{SZ}(b_\perp) \approx \frac{k_B\,T_e}{m_e\,c^2}\,\sigma_T\,\langle n_e\rangle\,L_{ICM} \tag{9}$$

$$\mathrm{DM}_{ICM}(b_\perp) \approx \langle n_e\rangle\,L_{ICM}, \tag{10}$$

where L_{ICM} is the line-of-sight lengthscale of the cluster at that $b_\perp$. By taking their ratio and re-arranging we can make a crude approximation for the mean plasma temperature at that physical offset,

$$\langle T_e(b_\perp)\rangle \approx \frac{m_e\,c^2}{\sigma_T\,k_B}\,\frac{y_{sz}}{\mathrm{DM}_{ICM}} \tag{11}$$

$$= 1.15\times10^7\,\mathrm{K}\left(\frac{y_{SZ}}{10^{-6}}\right)\left(\frac{\mathrm{DM}}{250\,\frac{\mathrm{pc}}{\mathrm{cm^3}}}\right)^{-1} \tag{12}$$

We estimate the projected y_{sz} at each cluster's $b_\perp$ from our fits to the Planck data described in Section 2. This gives $y_{SZ} = (3.31 \pm 1.36)\times10^{-6}$ for Abell 2310 at 520 kpc and $y_{SZ} = (6.80 \pm 3.03)\times10^{-7}$ for Abell 2311 at 870 kpc. Plugging these values into Eq. 12, we find $\langle k_B\,T_e\rangle \approx 0.8 - 3.9\,\mathrm{keV}$ for Abell 2310, in agreement with the expected electron temperature for a cluster of similar mass at that impact parameter (Vikhlinin et al. 2005; Pratt et al. 2007). This is the first time halo gas temperature has been measured using fast radio bursts. For Abell 2311 at 870 kpc we find $\langle k_B\,T_e\rangle \approx 0.6-16\,\mathrm{keV}$ along that line of sight. The large range in temperature is primarily due to the uncertainty in ICM DM for FRB 20220509G.

While it is hard to match the statistical precision of an X-ray spectroscopic temperature measurement, there are benefits to using FRB DMs to derive gas temperature: With FRBs we do not need to account for "clumping" effects due to the n_e^2 dependence (Eckert et al. 2015), the temperature will be approximately mass-weighted rather than the more complicated weighting intrinsic to spectroscopic measurements (Mazzotta et al. 2004), and current X-ray facilities are generally not sensitive beyond $\sim R_{500}$. The obvious drawbacks of using FRBs are that we have only a single sightline and the DM contribution of the IGM, Milky Way, and the host galaxy must be modelled. The former will be alleviated by FRB surveys with high areal density, providing multiple sightlines through individual halos. The latter may be aided by cross-correlation (e.g. (Madhavacheril et al. 2019; chi 2021)), which are less sensitive to host DM contamination. In Section 5 we describe how future surveys will allow for statistical FRB/cluster studies.

4. ILLUSTRISTNG CLUSTER SIMULATIONS

We use the IllustrisTNG simulation TNG300-1 (Nelson et al. 2019) to estimate typical DM values of the ICM as a function of impact parameter. We seek also to estimate the variance between galaxy clusters of similar mass, and variance within a cluster for different position angle at fixed impact parameter.

We first extract cylinders of length 300 Mpc and radius 5 Mpc from the simulation box that contain massive halos. These allow us to estimate not only the ICM contribution to DM, but also the IGM along that sightline.

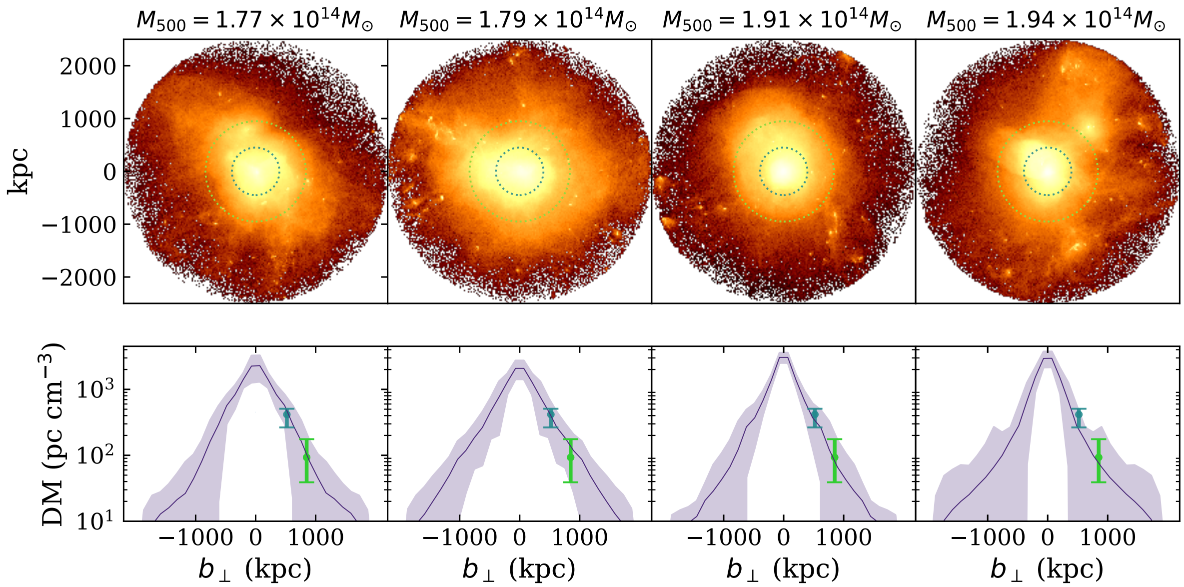


Figure 6. Four galaxy clusters from the TNG300-1 simulation whose masses are similar to those of Abell 2310 and Abell 2311. The top row show gas surface density within 2 Mpc of the cluster center. The green and blue circles represent the impact parameter of FRB 20220509G and FRB 20220914A, respectively. The bottom row shows $\mathrm{DM_{ICM}}$ as a function of impact parameter, $b_\perp$, with error bars for the two observed cluster FRBs. The solid purple line is the median DM over fifty azimuthal angles and the shaded region shows the 90% limits at that $b_\perp$. The curves assume the FRB is embedded halfway in the ICM, i.e. $l_{LOS} = 0$.

We then calculate gas properties for each cell in that cylinder and estimate free electron density as,

$$n_e = f_e\,\rho_g\,X_H\,/m_p, \tag{13}$$

where f_e is the free electron abundance, ρ_g is gas density, X_H is hydrogen abundance, and m_p is the proton mass. We take X_H to be 0.75. The ith cell's contribution to the total DM is,

$$\mathrm{DM}_i = n_e^i\,\Delta r_i\,(1+z_i)^{-1}, \tag{14}$$

where Δr_i is the distance through the cell at an impact parameter b_i. The cell's redshift is z_i. For cellsize, Δx, $\Delta r_i = 2\sqrt{\Delta x^2 - b_i^2}$. The total DM is then ΣDM_i for all cells that are intersected by the FRB.

We compute DM profiles for all halos in TNG300-1 that have $M_{500} > 10^{13.5}\,M_\odot$. In Figure 6 we show four galaxy clusters with masses comparable to the masses of host clusters of FRB 20220509G and FRB 20220914A. The blue and green data points in the bottom row correspond to the estimated ICM contribution to the two FRB DMs, which agree well with the expected range at their respective impact parameters. There is significant variance within a cluster even at a fixed impact parameter, particularly beyond the virial radius (corresponding to ≈ 1500 kpc given $R_{500} \approx 800$ kpc for these clusters). There is also some scatter between clusters, but the DM curves are roughly consistent. The mean values in DM vs. $b_\perp$ (solid purple lines in Figure 6) are also in agreement with analytic models for the cluster gas density (Vikhlinin et al. 2005; Prochaska & Zheng 2019).

Compared to simulations of the CGM or gas in galaxy groups, cluster simulations are in relatively good agreement with one another as well as with observations (Oppenheimer et al. 2021). As the sophistication of cosmological MHD simulations progresses, they will be an invaluable tool for understanding the properties of FRBs that are impacted by cluster gas. This is especially true for magnetic field inference from FRB RMs and for gas temperatures outside of R_{500}, as outlined in the following section.

5. DISCUSSION

5.1. *Beyond the virial radius*

Outside of the virial radii of galaxy clusters, plasma is difficult to observe via X-ray. FRB DMs, however, are more sensitive to this gas due to the n_e (rather than n_e^2) dependence, and can constrain to ICM and WHIM on the outskirts of clusters. Fujita et al. (2017) have shown that by combining FRB DMs with the pressure

profiles from SZ observations, the temperature profile of the WHIM can be obtained beyond $1.5\,R_{200}$.

In future FRB surveys, large numbers of localized FRBs will produce DM maps with high areal density, intersecting individual clusters along multiple sightlines. For example, the proposed DSA-2000 survey will spend roughly 5% of its time on deep-drilling fields that overlap with Rubin, XMM-LSS, Extended Chandra Deep Field-South, COSMOS deep fields (Hallinan et al. 2019b). This will lead to roughly 500 FRBs in just $\sim 10\,\mathrm{deg}^2$. Nearly every massive galaxy cluster out to $z = 0.3$ will be intersected by at least one FRB sightline. We will have a wealth of multiwavelength data in this field, including SZ data and deep X-ray observations. Such a dataset will allow us to constrain the magnetic field in the ICM and the density profile in the WHIM, as well as gas temperatures outside of R_{500}. However, from Figure 6 we see substantial azimuthal and inter-cluster variance in DM at large radii. Analyses of the gas beyond R_{500} ought to be done in tandem with cosmological MHD simulations.

5.2. *Prevalence of cluster FRBs*

Roughly 5% of sightlines from FRBs at $z \approx 0.5$ are expected to intersect galaxy clusters in the foreground (Prochaska & Zheng 2019). However, if an FRB sightline has a projected offset from a cluster that is less than R_{200}, it is more likely that the FRB came from the cluster itself than from behind it, assuming the rate of FRBs is related to stellar mass and not just star formation. This is because the overdensity of galaxies within massive halos is enough to counter the larger volume behind the galaxy cluster. Using $R_{200} \approx 1\,\mathrm{Mpc}$, the comoving volume in region of a cone behind a redshift 0.25 cluster out to $z = 0.5$ is $\sim 7 \times 10^3\,\mathrm{Mpc}^3$. Assuming a galaxy number density of roughly $10^{-2}\,\mathrm{Mpc}^{-3}$ (White et al. 2011), the volume behind the cluster should have only $\mathcal{O}(70)$ galaxies, compared with 10^{2-3} galaxies in the cluster. We note again that this rough estimate assumes cluster galaxies are as likely as non-cluster galaxies to produce FRBs. We have also ignored luminosity function considerations, which make FRBs behind the cluster to be more difficult to detect because they are less bright. It is therefore unsurprising that the first two localized FRBs that are known to be impacted by the ICM have come from member galaxies of clusters and not from behind clusters.

We have cross-matched twelve sources localized by the DSA-110 with cluster catalogs and found two FRBs that reside in galaxy clusters. This suggests the fraction of FRBs from galaxy clusters is $f_{cFRB} = 0.17^{+0.36}_{-0.12}$, using a 90% Poissonian confidence interval. We do not include other localized FRBs because we are not aware of concerted efforts to cross-match those FRB positions with clusters.

The large value of f_{cFRB} has interesting implications for FRBs detected at other surveys, and on our interpretation of observables such as the FRB DM distribution. CHIME/FRB detects $\mathcal{O}(10^3)$ FRBs per year, without sufficient localization precision to identify a host galaxy. They may therefore already have detected hundreds of sources that reside in galaxy clusters. The host ICM could then dominate the high-DM tail of the total observed DM distribution (James et al. 2022), which would otherwise be interpreted as the most distant sources. Even with arcminute localizations, a careful statistical cross-match of CHIME/FRB sources with galaxy cluster catalogs could reveal this signal.

5.3. *FRB progenitor implications*

FRB 20220509G is the first source to belong to an early-type galaxy. This fits an emerging picture that FRBs can be produced in a variety of environments, including dense star forming regions, globular clusters, and pristine environments with little HII (Tendulkar et al. 2017; Marcote et al. 2020; Pastor-Marazuela et al. 2021; Kirsten et al. 2022; Niu et al. 2022b). The full implications of FRB 20220509G's quiescent host will be fleshed out by Sharma et al. (in prep.). If more FRBs are localized to cluster galaxies with low rates of star formation, then progenitor models must explain evolutionary channels that can produce FRBs in the absence of recent core-collapse supernovae. This would be promising for FRB applications research, as early-type galaxies are not expected to have significant magnetoionic plasma in their ISM or HII regions near the source, alleviating the problem of disentangling host DM, RM, and scattering from cosmological contributions.

6. CONCLUSION

We have discovered two fast radio bursts sources that reside in massive galaxy clusters. The host galaxy of FRB 20220914A is a member of cluster Abell 2310, whose ICM dominates the DM budget of the FRB. We have combined the DM of FRB 20220914A with SZ observations of Abell 2310 to make the first estimate of the mean line-of-sight temperature of gas using an FRB. FRB 20220509G belongs to an early-type galaxy (Sharma et al., in prep.) at a projected offset of 870 kpc from the center of cluster Abell 2311. That cluster's ICM is found to contribute 16–172 $\mathrm{pc\,cm}^{-3}$ to the FRB DM, which is consistent with analytic models and simulations of the ICM for a cluster with mass $M_{500} \approx 1.5 - 2 \times 10^{14} M_{\odot}$. Polarization analysis of the

burst found significant Faraday rotation. Assuming this RM originates in the ICM, we constrain the mean line-of-sight magnetic field strength to be 0.75-7 μG in the intracluster gas. Roughly 17% of our first sample of localized FRBs were found to reside in galaxy clusters. While we expect this fraction to come down with time, galaxy clusters will likely play a significant role in upcoming FRB surveys, particularly in attempts at mapping out the Universe's baryons.

The authors thank staff members of the Owens Valley Radio Observatory and the Caltech radio group, including Kristen Bernasconi, Stephanie Cha-Ramos, Sarah Harnach, Tom Klinefelter, Lori McGraw, Corey Posner, Andres Rizo, Michael Virgin, Scott White, and Thomas Zentmyer. Their tireless efforts were instrumental to the success of the DSA-110. The DSA-110 is supported by the National Science Foundation Mid-Scale Innovations Program in Astronomical Sciences (MSIP) under grant AST-1836018. We acknowledge use of the VLA calibrator manual and the radio fundamental catalog. Some of the data presented herein were obtained at the W. M. Keck Observatory, which is operated as a scientific partnership among the California Institute of Technology, the University of California and the National Aeronautics and Space Administration. The Observatory was made possible by the generous financial support of the W. M. Keck Foundation. We thank Ryuichi Takahashi and Weiwei Xu for helpful discussions and materials related to their overlapping work. We also thank Nicholas Battaglia for useful discussion.

Facility: Keck:I (LRIS), Keck:II (ESI)

Software: astropy, CASA, frb, heimdall, lpipe, pPXF, Prospector, wsclean

REFERENCES

2021, 922, 42, doi: 10.3847/1538-4357/ac1dab

Abell, G. O. 1958, ApJS, 3, 211, doi: 10.1086/190036

Agarwal, D., Lorimer, D. R., Fialkov, A., et al. 2019, MNRAS, 490, 1, doi: 10.1093/mnras/stz2574

Anna-Thomas, R., Connor, L., Burke-Spolaor, S., et al. 2022, arXiv e-prints, arXiv:2202.11112. https://arxiv.org/abs/2202.11112

Arnaud, M., Pratt, G. W., Piffaretti, R., et al. 2010, A&A, 517, A92, doi: 10.1051/0004-6361/20091341610.48550/arXiv.0910.1234

Beniamini, P., Kumar, P., & Narayan, R. 2022, MNRAS, 510, 4654, doi: 10.1093/mnras/stab3730

Bhandari, S., Sadler, E. M., Prochaska, J. X., et al. 2020, ApJL, 895, L37, doi: 10.3847/2041-8213/ab672e

Bhardwaj, M., Gaensler, B. M., Kaspi, V. M., et al. 2021, ApJL, 910, L18, doi: 10.3847/2041-8213/abeaa6

Böhringer, H., Chon, G., & Kronberg, P. P. 2016, A&A, 596, A22, doi: 10.1051/0004-6361/201628873

Böhringer, H., & Werner, N. 2010, A&A Rv, 18, 127, doi: 10.1007/s00159-009-0023-3

Budzynski, J. M., Koposov, S. E., McCarthy, I. G., McGee, S. L., & Belokurov, V. 2012, MNRAS, 423, 104, doi: 10.1111/j.1365-2966.2012.20663.x

Carilli, C. L., & Taylor, G. B. 2002, ARA&A, 40, 319, doi: 10.1146/annurev.astro.40.060401.093852

Chambers, K. C., Magnier, E. A., Metcalfe, N., et al. 2016, arXiv e-prints, arXiv:1612.05560, doi: 10.48550/arXiv.1612.05560

Chatterjee, S., Law, C. J., Wharton, R. S., et al. 2017, Nature, 541, 58, doi: 10.1038/nature20797

CHIME/FRB Collaboration, Andersen, B. C., Bandura, K., et al. 2019, ApJL, 885, L24, doi: 10.3847/2041-8213/ab4a80

CHIME/FRB Collaboration, Amiri, M., Andersen, B. C., et al. 2021, ApJS, 257, 59, doi: 10.3847/1538-4365/ac33ab

Connor, L., & Ravi, V. 2022, Nature Astronomy, 6, 1035, doi: 10.1038/s41550-022-01719-7

Connor, L., Sievers, J., & Pen, U.-L. 2016, MNRAS, 458, L19, doi: 10.1093/mnrasl/slv124

Cook, A. M., Bhardwaj, M., Gaensler, B. M., et al. 2023, arXiv e-prints, arXiv:2301.03502, doi: 10.48550/arXiv.2301.03502

Cordes, J. M., & Chatterjee, S. 2019, ARA&A, 57, 417, doi: 10.1146/annurev-astro-091918-104501

Cordes, J. M., & Lazio, T. J. W. 2002, arXiv e-prints, astro. https://arxiv.org/abs/astro-ph/0207156

Dey, A., Schlegel, D. J., Lang, D., et al. 2019, AJ, 157, 168, doi: 10.3847/1538-3881/ab089d

Eckert, D., Molendi, S., Vazza, F., Ettori, S., & Paltani, S. 2013, A&A, 551, A22, doi: 10.1051/0004-6361/201220402

Eckert, D., Roncarelli, M., Ettori, S., et al. 2015, MNRAS, 447, 2198, doi: 10.1093/mnras/stu2590

Eckert, D., Ghirardini, V., Ettori, S., et al. 2019, A&A, 621, A40, doi: 10.1051/0004-6361/201833324

Fujita, Y., Akahori, T., Umetsu, K., Sarazin, C. L., & Wong, K.-W. 2017, ApJ, 834, 13, doi: 10.3847/1538-4357/834/1/13

Ghirardini, V., Eckert, D., Ettori, S., et al. 2019, A&A, 621, A41, doi: 10.1051/0004-6361/201833325

Hallinan, G., Dong, D., & Ravi, V. 2019a, The Astronomer's Telegram, 13018, 1

Hallinan, G., Ravi, V., Weinreb, S., et al. 2019b, in Bulletin of the American Astronomical Society, Vol. 51, 255. https://arxiv.org/abs/1907.07648

Heintz, K. E., Prochaska, J. X., Simha, S., et al. 2020, ApJ, 903, 152, doi: 10.3847/1538-4357/abb6fb

Hitomi Collaboration, Aharonian, F., Akamatsu, H., et al. 2016, Nature, 535, 117, doi: 10.1038/nature18627

Hutschenreuter, S., Anderson, C. S., Betti, S., et al. 2022, A&A, 657, A43, doi: 10.1051/0004-6361/202140486

James, C. W., Prochaska, J. X., Macquart, J. P., et al. 2022, MNRAS, 509, 4775, doi: 10.1093/mnras/stab3051

Kirsten, F., Marcote, B., Nimmo, K., et al. 2022, Nature, 602, 585, doi: 10.1038/s41586-021-04354-w

Lee, K.-G., Ata, M., Khrykin, I. S., et al. 2022, ApJ, 928, 9, doi: 10.3847/1538-4357/ac4f62

Lees, J. F. 1992, Publications of the Astronomical Society of the Pacific, 104, 154, doi: 10.1086/132971

Macquart, J. P., Prochaska, J. X., McQuinn, M., et al. 2020, Nature, 581, 391, doi: 10.1038/s41586-020-2300-2

Madhavacheril, M. S., Battaglia, N., Smith, K. M., & Sievers, J. L. 2019, PhRvD, 100, 103532, doi: 10.1103/PhysRevD.100.103532

Marcote, B., Nimmo, K., Hessels, J. W. T., et al. 2020, Nature, 577, 190, doi: 10.1038/s41586-019-1866-z

Marinacci, F., Vogelsberger, M., Pakmor, R., et al. 2018, MNRAS, 480, 5113, doi: 10.1093/mnras/sty2206

Masui, K., Lin, H.-H., Sievers, J., et al. 2015, Nature, 528, 523, doi: 10.1038/nature15769

Mazzotta, P., Rasia, E., Moscardini, L., & Tormen, G. 2004, MNRAS, 354, 10, doi: 10.1111/j.1365-2966.2004.08167.x

McQuinn, M. 2016, ARA&A, 54, 313, doi: 10.1146/annurev-astro-082214-122355

Mroczkowski, T., Nagai, D., Basu, K., et al. 2019, SSRv, 215, 17, doi: 10.1007/s11214-019-0581-2

Nelson, D., Springel, V., Pillepich, A., et al. 2019, Computational Astrophysics and Cosmology, 6, 2, doi: 10.1186/s40668-019-0028-x

Niu, C. H., Aggarwal, K., Li, D., et al. 2022a, Nature, 606, 873, doi: 10.1038/s41586-022-04755-5

—. 2022b, Nature, 606, 873, doi: 10.1038/s41586-022-04755-5

Ocker, S. K., Cordes, J. M., Chatterjee, S., & Gorsuch, M. R. 2022, ApJ, 934, 71, doi: 10.3847/1538-4357/ac75ba

Ocker, S. K., Cordes, J. M., Chatterjee, S., et al. 2023, MNRAS, 519, 821, doi: 10.1093/mnras/stac3547

Oppenheimer, B. D., Babul, A., Bahé, Y., Butsky, I. S., & McCarthy, I. G. 2021, Universe, 7, 209, doi: 10.3390/universe7070209

Pastor-Marazuela, I., Connor, L., van Leeuwen, J., et al. 2021, Nature, 596, 505, doi: 10.1038/s41586-021-03724-8

Petroff, E., Hessels, J. W. T., & Lorimer, D. R. 2019, A&A Rv, 27, 4, doi: 10.1007/s00159-019-0116-6

Petroff, E., Barr, E. D., Jameson, A., et al. 2016, PASA, 33, e045, doi: 10.1017/pasa.2016.35

Piffaretti, R., Arnaud, M., Pratt, G. W., Pointecouteau, E., & Melin, J. B. 2011, A&A, 534, A109, doi: 10.1051/0004-6361/201015377

Planck Collaboration, Ade, P. A. R., Aghanim, N., et al. 2014, A&A, 571, A20, doi: 10.1051/0004-6361/201321521

—. 2016a, A&A, 594, A27, doi: 10.1051/0004-6361/201525823

Planck Collaboration, Aghanim, N., Arnaud, M., et al. 2016b, A&A, 594, A22, doi: 10.1051/0004-6361/20152582610.48550/arXiv.1502.01596

Planck Collaboration, Ade, P. A. R., Aghanim, N., et al. 2016c, A&A, 596, A101, doi: 10.1051/0004-6361/201527743

Pratt, G. W., Böhringer, H., Croston, J. H., et al. 2007, A&A, 461, 71, doi: 10.1051/0004-6361:20065676

Pratt, G. W., Croston, J. H., Arnaud, M., & Böhringer, H. 2009a, A&A, 498, 361, doi: 10.1051/0004-6361/200810994
—. 2009b, A&A, 498, 361, doi: 10.1051/0004-6361/200810994
Prochaska, J. X., & Zheng, Y. 2019, MNRAS, 485, 648, doi: 10.1093/mnras/stz261
Ravi, V. 2019, ApJ, 872, 88, doi: 10.3847/1538-4357/aafb30
Ravi, V., Catha, M., D'Addario, L., et al. 2019, Nature, 572, 352, doi: 10.1038/s41586-019-1389-7
Ravi, V., Catha, M., Chen, G., et al. 2022, arXiv e-prints, arXiv:2211.09049, doi: 10.48550/arXiv.2211.09049
—. 2023, arXiv e-prints, arXiv:2301.01000. https://arxiv.org/abs/2301.01000
Sarazin, C. L. 1986, Reviews of Modern Physics, 58, 1, doi: 10.1103/RevModPhys.58.1
Sayers, J., Golwala, S. R., Mantz, A. B., et al. 2016, ApJ, 832, 26, doi: 10.3847/0004-637X/832/1/26
Seta, A., Rodrigues, L. F. S., Federrath, C., & Hales, C. A. 2021, ApJ, 907, 2, doi: 10.3847/1538-4357/abd2bb
Simard, D., & Ravi, V. 2021, arXiv e-prints, arXiv:2107.11334. https://arxiv.org/abs/2107.11334
Tendulkar, S. P., Bassa, C. G., Cordes, J. M., et al. 2017, ApJL, 834, L7, doi: 10.3847/2041-8213/834/2/L7
Tumlinson, J., Peeples, M. S., & Werk, J. K. 2017, ARA&A, 55, 389, doi: 10.1146/annurev-astro-091916-055240
van Weeren, R. J., de Gasperin, F., Akamatsu, H., et al. 2019, SSRv, 215, 16, doi: 10.1007/s11214-019-0584-z
Vikhlinin, A., Markevitch, M., Murray, S. S., et al. 2005, ApJ, 628, 655, doi: 10.1086/431142
Voit, G. M. 2005, Reviews of Modern Physics, 77, 207, doi: 10.1103/RevModPhys.77.207
White, D. J., Daw, E. J., & Dhillon, V. S. 2011, Classical and Quantum Gravity, 28, 085016, doi: 10.1088/0264-9381/28/8/085016
Xu, W., Ramos-Ceja, M. E., Pacaud, F., Reiprich, T. H., & Erben, T. 2022, A&A, 658, A59, doi: 10.1051/0004-6361/202140908
Yang, X., Xu, H., He, M., et al. 2021, ApJ, 909, 143, doi: 10.3847/1538-4357/abddb2
Yao, J. M., Manchester, R. N., & Wang, N. 2017, ApJ, 835, 29, doi: 10.3847/1538-4357/835/1/29
Zhang, Z. J., Yan, K., Li, C. M., Zhang, G. Q., & Wang, F. Y. 2021, ApJ, 906, 49, doi: 10.3847/1538-4357/abceb9